Poloidal Rotation Dynamics, Radial Electric Field, and Neoclassical Theory in the Jet Internal-Transport-Barrier Region

K. Crombé,[1] Y. Andrew,[2] M. Brix,[3] C. Giroud,[2] S. Hacquin,[4] N. C. Hawkes,[2] A. Murari,[5] M. F. F. Nave,[4] J. Ongena,[6] V. Parail,[2] G. Van Oost,[1] I. Voitsekhovitch,[2] and K.-D. Zastrow[2]

[1]*Department of Applied Physics, Ghent University, Belgium*
[2]*Euratom/UKAEA, Fusion Association, Culham Science Center, Oxon, UK*
[3]*Association EURATOM-FZ-Jülich, Institut für Plasmaphysik, Jülich, Germany*
[4]*Associação EURATOM/IST, Centro de Fusão Nuclear, Lisbon, Portugal*
[5]*Consorzio RFX, ENEA-Euratom Association, Padua, Italy*
[6]*LPP/ERM-KMS, Association EURATOM-Belgian State, B-1000 Brussels, Belgium*

(Received 14 April 2005; published 7 October 2005)

Results from the first measurements of a core plasma poloidal rotation velocity (v_θ) across internal transport barriers (ITB) on JET are presented. The spatial and temporal evolution of the ITB can be followed along with the v_θ radial profiles, providing a very clear link between the location of the steepest region of the ion temperature gradient and localized spin-up of v_θ. The v_θ measurements are an order of magnitude higher than the neoclassical predictions for thermal particles in the ITB region, contrary to the close agreement found between the determined and predicted particle and heat transport coefficients [K.-D. Zastrow *et al.*, Plasma Phys. Controlled Fusion **46**, B255 (2004)]. These results have significant implications for the understanding of transport barrier dynamics due to their large impact on the measured radial electric field profile.

DOI: 10.1103/PhysRevLett.95.155003 PACS numbers: 52.55.Fa, 52.25.Fi, 52.30.−q, 52.70.Kz

The internal transport barrier (ITB) regime is an advanced operation scenario presently studied on JET with a view to its extension to next step, large fusion devices. A great deal of progress has been made in recent years in the theoretical modeling [1–5] and experimental control [6–8] of ITBs. However the underlying mechanisms for ITB formation and sustainment are not yet fully understood. Turbulence suppression in the region of the ITB is thought to be controlled by the interaction of different physical mechanisms of which there are several commonly studied aspects. These include a sheared $\mathbf{E} \times \mathbf{B}$ flow that stabilizes ion or electron temperature gradient modes or trapped electron modes [9–11] (and references therein). Another important factor is thought to be the q profile: (a) a low or negative magnetic shear influences the growth rate of the instabilities [3,6–12], (b) the low order rational q surfaces favorably stabilize $\mathbf{E} \times \mathbf{B}$ flow shear [3,10,11], and (c) strongly reversed q helps α stabilization [13,14]. Additional factors that have also been considered include the ion to electron temperature ratio (T_i/T_e) [10,11,15], strong electron density gradients [2], and turbulence driven self-generated zonal flows [16–18]. The focus for this Letter is on turbulence suppression through sheared $\mathbf{E} \times \mathbf{B}$ flow with the evolution of measured core plasma v_θ and radial electric field (E_r) profiles in the barrier region on JET. Using the force balance equation, E_r can be written as

$$E_r = \frac{\nabla p}{neZ} + v_\phi B_\theta - v_\theta B_\phi \qquad (1)$$

where p is the ion pressure, Z the ion charge number, e the elementary charge, n is the ion density, v_ϕ and v_θ are the ion toroidal and poloidal rotation velocities, respectively, and B_θ and B_ϕ are the poloidal and toroidal magnetic fields. This expression for E_r is valid for each of the different fuel and impurity ion species individually. On JET the pressure profile and rotation velocities are measured using charge eXchange recombination spectroscopy (CXRS) [19,20] for the carbon ions and all quantities in Eq. (1) in this study refer to C^{6+} ions. The poloidal CXRS system simultaneously records spectra along six viewing chords [19,21], which are selected on a shot-to-shot basis. For the studies of ITB plasmas the midplane radii of the channels are in the range $R_{mid} = 3.30$–3.65 m. The angle between the chords of the poloidal system and the toroidal (poloidal) direction is about 80° (15°), whereas the angle between the beam line and observation direction is about 75°. The toroidal rotation velocity is measured by a toroidal CXRS system (with purely toroidal view). For the calculation of v_θ the toroidal component is subtracted from the total measured velocity along the poloidal lines of sight [19,21]. The poloidal CXRS system views the pinis 4 and 6 of the octant 4 neutral beam and the toroidal CXRS system views the pinis 6 and 7 of the octant 8 neutral beam.

The first shot considered (No. 61352), is a typical ITB plasma with negative central shear in which deuterium and tritium gas fueling was used [22]. For this discharge 13 MW of neutral beam injection, 4 MW of ion cyclotron range of frequency, and 2 MW of lower hybrid heating were applied. The T_i profiles for time slices during the formation and radial expansion of the ITB are shown in Fig. 1(a). The ITB criterion for this shot is shown in

Fig. 2(a) to further illustrate the temporal and spatial evolution of the transport barrier. The ITB criterion is defined here as when the local dimensionless Larmor radius (ρ_T^*), with $\rho_T^* = \rho_S/L_T$ (the ratio of the Larmor radius at the sound speed, ρ_S, and the local temperature gradient scale length, L_T), exceeds a critical value of 0.014 as described in [23]. The spatial location of three of the CXRS viewing channels are indicated in Figs. 1(a) and 2(a). The radial extent of the intersection of the CXRS channels and the beam injection is about 8 cm for the inner chords and decreases to about 5 cm for the outer chords. This spatial resolution is determined by the line integration through the finite beam injection volume and the finite spot size of the optical fibres at the intersection with the beam. The corresponding v_θ time traces for each of these channels are shown in Fig. 2(b). The value of v_θ for the line of sight at the magnetic midplane $R_{\text{mid}} = 3.33$ m increases in the positive (electron diamagnetic) direction, from 7 to 20 km/s during the time that the channel views the center of the steep T_i gradient ($t \sim 4.0$–5.1 s). As the barrier moves outwards ($t > 5.1$ s) the relative location of the v_θ measurements change with respect to the T_i gradient, and a strong positive increase in v_θ is picked up by the adjacent CXRS channel ($R_{\text{mid}} = 3.40$ m), increasing from 7 to 40 km/s. The innermost channel ($R_{\text{mid}} = 3.33$ m) simultaneously measures v_θ to change sign and spin-up to -25 km/s in the ion diamagnetic direction, resulting in a strong shear in poloidal rotation. The value of v_θ along the outermost channel, with a view outside the T_i gradient region ($R_{\text{mid}} = 3.46$ m) is constant at about 7 km/s throughout the discharge. In the final phase of the ITB evolution, the steep Ti gradient moves inwards once again at $t \sim 7.0$ s. As this happens v_θ at $R_{\text{mid}} = 3.40$ m returns to its initial value of $\sim$7 km/s and v_θ at R_{mid} increases back to 25 km/s in the electron diamagnetic direction.

A temperature correction has been included in the analysis for the v_θ measurements. This correction comprises both a term for the energy dependence of the charge exchange cross section using the approach of von Hellermann [24] and a correction for gyro-orbit motion during the finite lifetime of the exciting state [25], starting from the analytic expressions in [26], integrated along the CXRS lines of sight on JET. The energy dependence of the CX cross section has the largest implications on the measured profiles; for the innermost v_θ chord (where the T_i is the highest and thus these effects are the most important) the noncorrected velocity is up to 100% higher (in the positive direction). After correcting for the apparent line shift due to the gyro-orbit motion, the resulting experimental v_θ values are an additional 25% more negative.

Measurements of v_θ are also presented for a second shot (No. 58094) in which more centrally viewing CXRS channels were used, as indicated in Fig. 1(b). In this plasma the central T_i was higher than in the previous example, with values up to 24 keV in the center [Fig. 1(b)]. The temporal and spatial evolution of the ITB along with the three v_θ channels covering the gradient region (from $R_{\text{mid}} = 3.28$ m to $R_{\text{mid}} = 3.46$ m are shown in Figs. 3(a) and 3(b). The measurements show v_θ to increase strongly to -75 km/s for the channel at $R_{\text{mid}} = 3.34$ m, when the central T_i reaches it highest values. This channel views the inner edge of the steep T_i gradient during this time. The innermost channel at $R_{\text{mid}} = 3.28$ m is located in a less steep part of the T_i gradient and shows a smaller negative increase to -40 km/s. The channel at $R_{\text{mid}} = 3.46$ m, which views the foot of the barrier, does not show any significant change in v_θ.

Reflectometry measurements obtained in the O-mode polarization for a probing frequency (36.9 GHz) are shown in Fig. 4 for this shot (No. 58094). The radial position of the cutoff layer for the probing frequency (39.6 GHz) and two other close frequencies (38.1 and 41.1 GHz) are shown

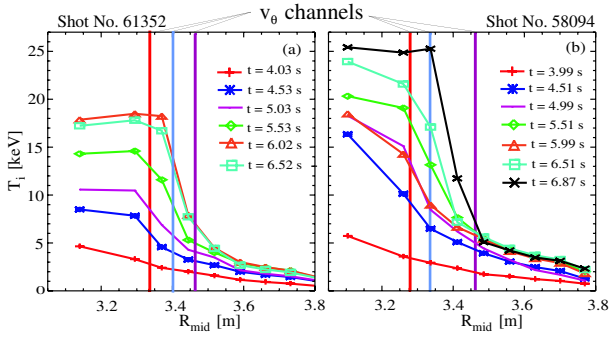

FIG. 1 (color online). Radial T_i profiles during the evolution of the ITB for (a) No. 61352 and (b) No. 58094. The vertical lines show the locations of the CXRS channels for v_θ measurements.

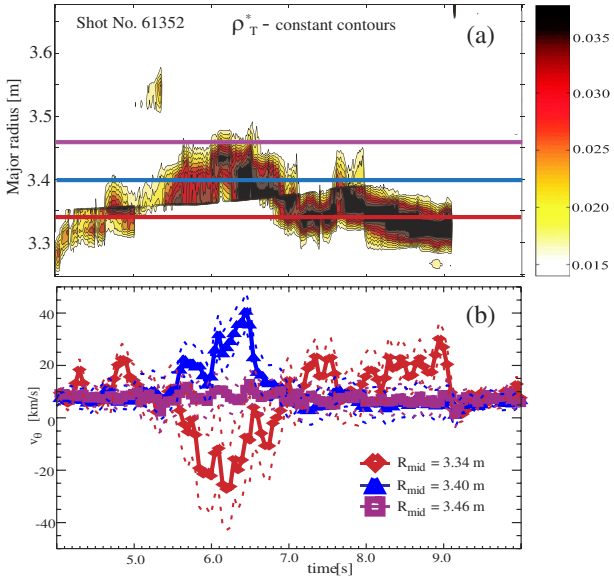

FIG. 2 (color online). (a) The ITB criterion and the locations of three of the v_θ channels in the region of the steep temperature gradient. (b) Time traces of v_θ at the three different CXRS radii shown in Fig. 2(a), with the error bars represented by the dotted curves.

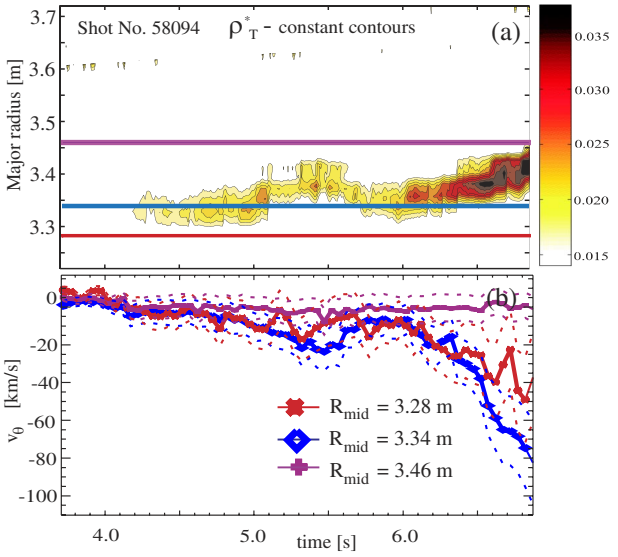

FIG. 3 (color online). (a) ITB criterion for shot No. 58094 and the locations of the CXRS channels for v_θ measurement. (b) Time traces of v_θ measured at the three different radii shown in Fig. 3(a).

in Fig. 4(a). The spectrogram computed from a sliding fast Fourier transform (FFT) of the reflected signal and the spectrogram integrated over the whole frequency range are depicted in Figs. 4(b) and 4(c), respectively. A reduction in the fluctuation level during $t = 5.0$–5.6 s and after $t = 6.0$ s can be seen, corresponding to the two time intervals with large negative v_θ excursions in the vicinity of the reflecting layer [as shown in Fig. 3(b)]. For the shot No. 61352, a reduction in the turbulent fluctuations was also observed during the increase in v_θ.

These two examples demonstrate a clear link between the existence of an ITB and large, localized excursions in v_θ on JET. A limited spatial coverage of the core region for poloidal rotation measurements ($R_{mid} = 3.30$ m, mostly corresponding to $\rho = 0.3$) and the fact that the barrier is often formed more centrally than the innermost viewing

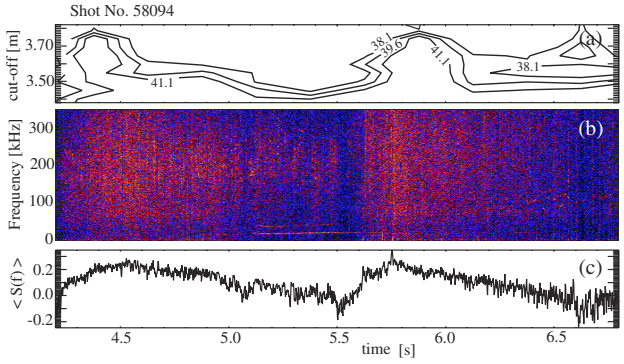

FIG. 4 (color online). Reflectometry measurements of (a) radial position of the cutoff layer for three frequencies, (b) sliding FFT spectrogram of the reflected signal and (c) integrated spectrogram.

chord, combined with a modest time resolution of 50 ms, means that it is not possible to resolve the question of causality between the ITB formation and v_θ excursions on JET. However, it is clear that the increase in v_θ persists throughout the duration of the barrier, and in this respect differs from the poloidal rotation precursors observed on the tokamak fusion test reactor (TFTR) [27,28]. As shown in Fig. 2, after the ITB disappears ($t > 9.0$ s) v_θ along the three inner chords relaxes back to pre-ITB values.

For the trace tritium plasma (No. 61352), the tritium transport coefficients, both the diffusion coefficient (D_T) and the convective velocity (v_T), were also determined and compared with their neoclassical estimations in [29]. A strong reduction in the particle transport coefficients was seen in the barrier region, to the neoclassical level for D_T and slightly above for v_T. The ion heat diffusivity χ_i was also found to reach the neoclassical level. The comparison between the CXRS measurements of v_θ and the neoclassical predictions for impurity and main ions by NCLASS [30] is shown in Figs. 5(a) and 5(b). The NCLASS predictions of v_θ are for thermal particles. The transport codes JETTO and TRANSP have been used to simulate the plasmas and both the measured and calculated v_θ profiles are compared at a single time slice during the barrier for the two shots described above. At the location of the negative dip in the neoclassical predictions, at around $\rho = 0.35$ ($R_{mid} = 3.33$ m), the largest negative v_θ values are measured. There appears however, to be a significant difference in absolute values of almost an order of magnitude. The positive increase for the channel around $\rho = 0.45$ ($R_{mid} = 3.40$ m) in discharge No. 61352, measured in the middle of the T_i gradient, is not reproduced by the NCLASS calculations. Comparison of the experimental profiles to the predictions for the main ion v_θ [Figs. 5(a) and 5(b)] shows

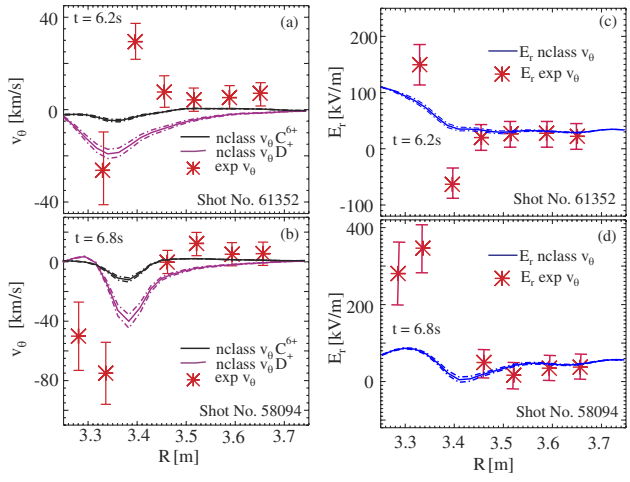

FIG. 5 (color online). (a) and (b) Comparison of measured v_θ profiles with neoclassical predictions for the thermal particles by NCLASS for the two discharges during the ITB. (c) and (d) E_r profiles calculated using Eq. (1), with the measured v_θ values (stars) and the NCLASS v_θ predictions (solid line) and measured toroidal and pressure gradient components.

relatively good agreement in absolute value for the excursion in the negative direction. The cause for the difference between measured and calculated v_θ is at present unclear; one possibility for this is that the effect of the parallel flow, driven by the fast beam ions, is not included in NCLASS [31,32]. However, for No. 58094 large differences between measured and calculated v_θ exist despite a constant beam power during the barrier evolution. The changes in beam deposition profile during the ITB evolution show no clear correlation with the evolution of the measured v_θ. In addition, large impurity ion v_θ values were reported in [32] during quiescent H-mode discharges on DIII-D, with similar values of central T_i to the JET ITB shots shown here.

Using the experimental v_θ values instead of the neoclassical predictions in the calculation of the total E_r field [from Eq. (1)], results in a significant difference in the region of the barrier, as is shown in Figs. 5(c) and 5(d)]. Outside the ITB ($R_{\text{mid}} > 3.40$ m) there is good agreement between the JETTO output and the fully experimental E_r. In the region of the steep pressure gradient however, the shear in E_r is significantly larger when the experimental v_θ values are used instead of the NCLASS predictions, suggesting that the stabilizing shear in the $\mathbf{E} \times \mathbf{B}$ flow is in fact stronger than the calculations predict. The poloidal term ($v_\theta B_\phi$) in E_r in these examples has the same order of magnitude as the large toroidal term ($v_\phi B_\theta$), which originates from the external momentum input by unidirectional neutral beam injection.

In conclusion, high poloidal rotation velocities closely related to barrier dynamics have been identified on JET, about an order of magnitude larger than the neoclassical predictions for thermal particles. The v_θ excursions are in different rotational directions, depending on the location of the measurement relative to the barrier. The time intervals, during which a reduction in turbulent fluctuations are observed, coincide with the large excursions in v_θ. The values of E_r in the barrier region are also considerably different if the measured v_θ profiles are used instead of neoclassical calculations, possibly affecting the calculation of the q profile.

The authors would like to thank Tuomas Tala for very helpful discussions. This work has been performed under the European Fusion Development Agreement (EFDA) and was funded partly by the Ghent University (Belgium), by the United Kingdom Engineering and Physical Sciences Research Council, and by the Euratom mobility. This work was done under the JET-EFDA workprogramme [33].

[1] T. Tala *et al.*, Plasma Phys. Controlled Fusion **43**, 507 (2001).
[2] T. Tala *et al.*, Plasma Phys. Controlled Fusion **44**, A495 (2002).
[3] Y. Baranov *et al.*, Plasma Phys. Controlled Fusion **46**, 1181 (2004).
[4] V. Parail *et al.*, Nucl. Fusion **39**, 429 (1999).
[5] T. Tala *et al.*, Nucl. Fusion, "Fully Predictive Transport Simulations of ITB Plasmas in JET, JT-60U and DIII-D" (to be published).
[6] C. Challis *et al.*, Plasma Phys. Controlled Fusion **43**, 861 (2001).
[7] C. Challis *et al.*, Plasma Phys. Controlled Fusion **44**, 1031 (2002).
[8] N. Hawkes *et al.*, Plasma Phys. Controlled Fusion **44**, 1105 (2002).
[9] K. Burrell *et al.*, Phys. Plasmas **4**, 1499 (1997).
[10] J. Connor *et al.*, Nucl. Fusion **44**, R1 (2004).
[11] R. Wolf, Plasma Phys. Controlled Fusion **45**, R1 (2003).
[12] N. Hawkes *et al.*, Phys. Rev. Lett. **87**, 115001 (2001).
[13] M. Beer *et al.*, Phys. Plasmas **4**, 1792 (1997).
[14] C. Bourdelle *et al.*, in *Proceedings of the 30th EPS Conference on Controlled Fusion and Plasma Physics, St. Petersburg, July 2003* (European Physical Society, Petit-Lancy, Switzerland, 2003); Europhys. Conf. Abstr. **27A**, 1.89 (2003).
[15] S. Ide, Phys. Plasmas **7**, 1927 (2000).
[16] Z. Lin *et al.*, Phys. Rev. Lett. **83**, 3645 (1999).
[17] B. Rogers *et al.*, Phys. Rev. Lett. **85**, 5336 (2000).
[18] T. Hahm *et al.*, Plasma Phys. Controlled Fusion **42**, A205 (2000).
[19] K. Crombé *et al.*, Rev. Sci. Instrum. **75**, 3452 (2004).
[20] M. von Hellermann *et al.*, Rev. Sci. Instrum. **61**, 3479 (1990).
[21] K. Crombé *et al.*, in *Proceedings of the 30th EPS Conference on Controlled Fusion and Plasma Physics, St. Petersburg, July 2003* (European Physical Society, Petit-Lancy, Switzerland, 2003); Europhys. Conf. Abstr. **27A**, 1.55 (2003).
[22] J. Mailloux *et al.*, in *Proceedings of the 31st EPS Conference on Conference on Controlled Fusion and Plasma Physics, London, June 2004* (European Physical Society, Petit-Lancy, Switzerland, 2004); Europhys. Conf. Abstr. **28G**, 1.148 (2004).
[23] G. Tresset *et al.*, Nucl. Fusion **42**, 520 (2002).
[24] M. von Hellermann *et al.*, Plasma Phys. Controlled Fusion **37**, 71 (1995).
[25] R. Bell *et al.*, AIP Conf. Proc. **547**, 39 (2000).
[26] W. Solomon *et al.*, Rev. Sci. Instrum. **75**, 3481 (2004).
[27] R. Bell *et al.*, Phys. Rev. Lett. **81**, 1429 (1998).
[28] G. Staebler *et al.*, Nucl. Fusion **41**, 891 (2001).
[29] K.-D. Zastrow *et al.*, Plasma Phys. Controlled Fusion **46**, B255 (2004).
[30] W. Houlberg *et al.*, Phys. Plasmas **4**, 3230 (1997).
[31] W. Houlberg *et al.*, "Accurate Calculation of Shielding Factor for High Energy Beam Currents" in *Proceedings of the 46th APS Conference, Savannah, Georgia, 2004.*
[32] W. Solomon *et al.*, *Proceedings of the 20th IAEA Fusion Energy Conference, Vilamoura, 2004* (IAEA, Vienna, 2005).
[33] J. Pamela *et al.*, *Fusion Energy 2004 (Proceedings of the 20th International Conference, Vilamoura, 2004)* [International Atomic Energy Agency (IAEA),Vienna, 2004]. (All the members of the JET-EFDA Collaboration appear in the appendix of this paper.)